X-RAY SPECTROMETRY, VOL. 16, 195-201 (1987)

# Analytic Description of Si(Li) Spectral Lineshapes Due to Monoenergetic Photons

**J. L. Campbell, A. Perujo and B. M. Millman**
Guelph Waterloo Program for Graduate Work in Physics, Department of Physics, University of Guelph, Guelph, Ontario, N1G 2W1, Canada

**Spectra have been recorded from monochromatized $K\alpha_1$, $K\beta_1$ and $L\alpha_1$ x-rays in the 3–16 keV energy region incident on an Si(Li) detector. An analytic lineshape consisting of a Gaussian plus two Gaussian-exponential convolutes fits these well, except at very low energy. The intensities and parameters of these tails are explored in the context of the processes responsible, and the behaviour of the shorter tail is compared with the predictions of a model calculation of Auger and photoelectron escape. The well behaved energy dependence of the tailing parameters improves the prospects for more accurate fitting of complex XRF, EPMA and PIXE spectra.**

## INTRODUCTION

Energy-dispersive x-ray analysis is widely used in analytical techniques such as XRF (x-ray fluorescence analysis), EPMA (electron probe microanalysis) and PIXE (proton-induced x-ray emission analysis). The spectrometer is invariably an Si(Li) detector. The low-energy tailing of peaks in Si(Li) x-ray spectra is a major source of uncertainty in the extraction of peak areas and hence elemental concentrations. It is desirable to have a convenient analytical form for the tails, which may simply be added to the Gaussian which represents the principal component of a peak; it is also desirable to understand the tailing in terms of the physical properties of the Si(Li) crystal.

In the 1-20 keV region there are several contributors to low-energy tailing. The relative importance of these is depicted very crudely in Fig. 1. Surface dead layers and other imperfections in the Si(Li) crystal produce tails whose intensity relative to the overall peak area falls very rapidly with increasing energy. Radiative Auger satellites lie just below the $K\alpha$ and $K\beta$ x-ray peaks of each element, and augment the observed 'tailing;' their intensities are strongly $Z$-dependent, resulting in energy dependences different from those of the tails caused by detector imperfections; also, the ratio of the $K\beta$ satellite (KMM) intensity to that of the $K\beta$ line is about an order of magnitude more intense than in the case of the $K\alpha$ satellites (KLM, KLL) and their parent line. Finally, as the photon energy reaches 15 keV, Compton scatter humps appear on the low-energy sides of peaks, their intensity growing with increasing energy and depending on the atomic number of the specimen emitting the x-rays.

If not recognized and catered for, these effects will at best worsen the chi-squared ($\chi^2_r$) fit when an energy-dispersive x-ray spectrum is fitted to a model, thereby decreasing the confidence of the recipient of the analytical results. At worst the fitting procedure may compensate by introducing small amounts of spurious elements. There is also an interplay between these effects and the approach adopted for modelling or stripping away the background continuum. If the background is fitted by a polynomial, these distortions will have maximum effect; however, since they are markedly less peaked than the principal (Gaussian) component, a frequency-sensitive filtering procedure may partially remove them.

Given the complexity of the overall tailing, it is very difficult to study the imperfection tailing using x-ray spectra; not only are all three tailing effects present but the spectra are multiplets and the three effects have different and strong energy dependences. We have therefore reported lineshape studies[1] using individual $K\alpha_1$ and $L\alpha_1$ lines selected by Bragg diffraction from a curved crystal. We fitted various analytic functions to peaks in the 2–25 keV region and found that the Hypermet function of Phillips and Marlowe,[2] originally intended for use with Ge(Li) gamma-ray spectrometers at energies over 100 keV, was the most appropriate.

In our previous work[1] we used a detector of modest energy resolution. We have now made a more detailed study with a detector of very good resolution, and this has led to various new results, which we present here.

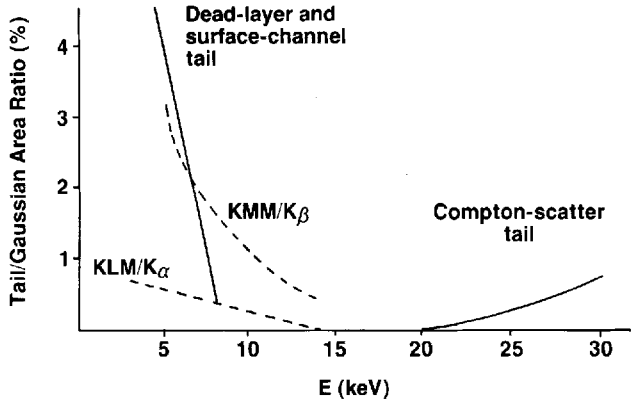


**Figure 1.** Energy dependence of tail/Gaussian intensity ratios for different spectral distortions in a particular Si(Li) detector; the data below 15 keV are quantitatively correct for the device studied here, whereas those above 15 keV are entirely qualitative. The continuous lines represent degradation processes and the dashed lines radiative Auger satellites.

0049-8246/87/050195-07 $05.00


*Received 4 December 1986*
*Accepted 4 April 1987*

## EXPERIMENTAL

The Si(Li) crystal used had a nominal diameter of 6 mm and a depth of 5 mm. The actual diameter, measured by scanning radially with a finely collimated Mn K x-ray beam from a 20 mCi $^{55}$Fe radionuclide source, was 5.62 mm. The beryllium window was 0.025 mm thick. A tantalum screen with a 4 mm diameter circular aperture limited photons to the central region of the detector.

Characteristic x-ray lines in the energy range 3–20 keV were derived from a Jarrell-Ash Model 80 microfocus x-ray generator (foreshortened beam 100 μm in diameter), fitted with a curved quartz crystal focusing monochromator. Crystals of length 4 cm and radii of curvature varying from 35 to 250 cm were used; Bragg reflections were taken from the 110 planes, the angle of which to the surface ranged from 1.5° to 6° depending on the particular crystal. The source-crystal and crystal-focus distances were 17–20 and 25–33 cm, respectively. A $0.120 \times 2$ mm slit was placed at the focus. To achieve a $5 \times 5$ mm beam at the Si(Li) detector, the latter was placed 75 cm from the slit. The region between the crystal and the detector was evacuated to minimize absorption losses and scattering; in the case of Ag Lα, the space not evacuated was filled with helium.

Counting rates were controlled by adjustment of the generator current and by interposing aluminium and/or brass foils between the anode and the diffracting crystal. Typical rates were 300–500 cps. The Ortec 572 amplifier used here provided pile-up rejection through anti-coincidence gating of the Nuclear Data 575 ADC. Digital stabilization was used, via an ND590 Spectrum Stabilizer. The integrated intensity of peaks was typically $5 \times 10^6$ counts.

## CHOICE OF ANALYTIC LINESHAPE FUNCTION

In our previous paper[1] we reviewed various lineshape functions from the literature. Each of these was, explicitly or implicitly, a variant on the form that we found to be most appropriate, namely the Hypermet function.[2] This is

$$F(i) = G(i) + S(i) + D(i) + E(i) \tag{1}$$

where $i$ represents channel number, and

$$G(i) = H_G \exp\left[-\frac{(i-i_0)^2}{2\sigma^2}\right] \tag{2}$$

$$S(i) = \tfrac{1}{2} H_S \operatorname{erfc}\left(\frac{i-i_0}{\sigma\sqrt{2}}\right) \tag{3}$$

$$D(i) = \tfrac{1}{2} H_D \exp\left(\frac{i-i_0}{\beta}\right) \operatorname{erfc}\left(\frac{i-i_0}{\sigma\sqrt{2}} + \frac{\sigma}{\beta\sqrt{2}}\right) \tag{4}$$

The $S$ and $D$ components are a flat shelf and an exponential tail, respectively, each convoluted with a unit-area Gaussian of width $\sigma$, to represent the observed distortion on the low-energy side of a peak.

Each peak in an Si(Li) spectrum is accompanied by an 'escape peak' $E(i)$ arising from the escape of silicon K x-rays following a photoelectric interaction in the K shell of a silicon atom near the detector surface. Previously we represented this by a second Gaussian, displaced leftward in energy by 1.742 keV, i.e. by the Si K-shell binding energy. In this work the lineshape $E(i)$ of the escape peak was investigated in more detail and its energy shift relative to its parent was found to be 1.752 keV.

No attempt is made here to convolute into the lineshape either the natural $K\alpha_1$ or $K\alpha_2$ linewidth or the slit transmission linewidth, both of which are negligible in comparison with the intrinsic resolution (full width at half maximum intensity, FWHM $= 2.35\sigma$) of the Si(Li) detector.

Discussion of the physical origin of the observed features $D$ and $S$ is delayed until later in this paper. We note here that if two or more distinct physical processes give rise to exponential tails, it is legitimate to use two or more tails of the form of $D$. However, the sum of two (or more) such tails might well provide an acceptable description of two (or more) processes whose individual response functions are other than exponential.

A polynomial model may be used to represent the continuum background and in our spectra, which are simple and extend over only small energy regions, a linear background,

$$B(i) = a + bi \tag{5}$$

suffices.

To determine the parameters of Eqns (2)–(5), the model spectrum $S(i) = F(i) + B(i)$ is fitted to the measured spectrum by conventional non-linear least-squares methodology.

For the sake of uniformity, we express all reduced chi-squared values ($\chi_r^2$) throughout this paper as corresponding to an intensity of $10^6$ counts in the fitted region. This is easily shown to be

$$\chi_r^2 = 1 + \frac{(\chi_r^2)_N - 1}{N} \tag{6}$$

where $(\chi_r^2)_N$ is the actual chi-squared achieved in fitting the measured spectrum containing $N \times 10^6$ counts. This approach eliminates potentially misleading comparisons of the goodness of fit for spectra of very different intensities.

## MONOENERGETIC PHOTON STUDIES

### Preliminaries

At the outset the electronic system was adjusted to minimize peak distortions. An amplifier time constant of 3 μs was chosen; although a larger value would have given slightly better energy resolution, the lengths of delay line needed in the pile-up rejection system would have become intolerably long. Using the copper $K\alpha_1$ line, several spectra were recorded as a function of amplifier pole-zero setting; from the fits to these, the pole-zero setting that afforded the minimum area of the

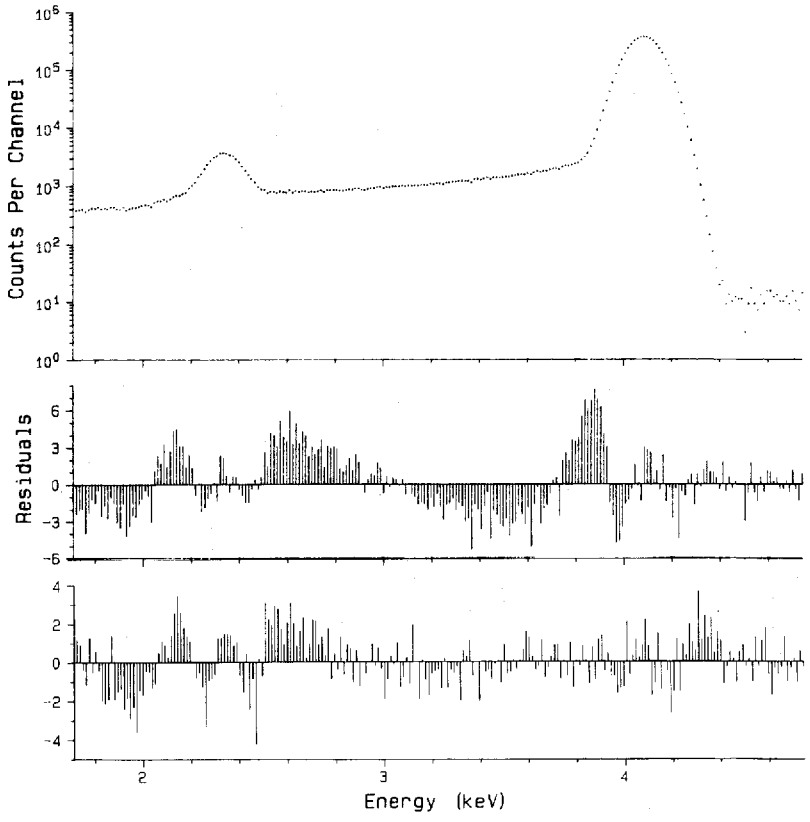


**Figure 2.** Results of test fits to the scandium K$\alpha_1$ line. The upper residues are for the model spectrum $G(i)+S(i)+D(i)+B(i)+E(i)$ and the lower residues are for the model spectrum $G(i)+B(i)+D_S(i)+D_L(i)+B(i)+E(i)$. The residues are weighted by the square root error of the counts per channel.

tail component relative to the Gaussian ($A_D/A_G$) was ascertained.

Preliminary measurements on the K$\alpha_1$ lines from Sc, Cr, Fe, Cu and Zr indicated that fits of Eqn (1) to the data, i.e. using a single tail $D(i)$, gave disappointing results. The residuals indicated failure to account for all of the low-energy tailing features, as shown for the Sc K$\alpha_1$ line in Fig. 2a. Introduction of a second exponential tail resulted in a major improvement (e.g. Fig. 2b). An important aspect of the two-tail fits was that the contribution from the flat shelf $S(i)$ became negligible; clearly two exponential tails represent the physical processes occurring with 4–15 keV photons better than one tail plus a shelf.

From here the analytic lineshape was taken to be

$$F(i)=G(i)+D_L(i)+D_S(i)+E(i) \qquad (7)$$

where the suffixes L and S signify long- and short-term, respectively.

In our previous work, where counting statistics were lower and the energy resolution slightly poorer, the escape peak $E(i)$ was given a Gaussian shape. Here this caused clear misfits. By definition, escape events arise close to the detector surface, where the probability of charge loss is greatest. One should therefore expect escape peaks to display strong low-energy tailing. As a first approximation to this effect we represented $E(i)$ here by a Gaussian with two tails whose height and slope parameters were equal to those of the parent peak. This resulted in improved fits in the escape peak region.

In order to choose the optimum collimation, Sc K$\alpha_1$ spectra were recorded with tantalum apertures of 2–6 mm diameter immediately in front of the Si(Li) detector. Figure 3 shows the dependence of the relative areas of the long and the short exponential tails on the exposed detector radius. Clearly both features increase in intensity near the periphery. We compromised between minimum tailing and efficient use of the detector by adopting a 4 mm aperture.

## Energy dependence of lineshape features

The K$\alpha_1$ lines of Sc, Cr, Fe, Cu and Zr and the K$\beta_1$ lines of Ge and Mo were recorded ($5\times10^6$ counts in each) to examine the energy region 4–20 keV. The quality of fits of Eqn (7) was excellent, with $\chi^2_\nu$ values per $10^6$

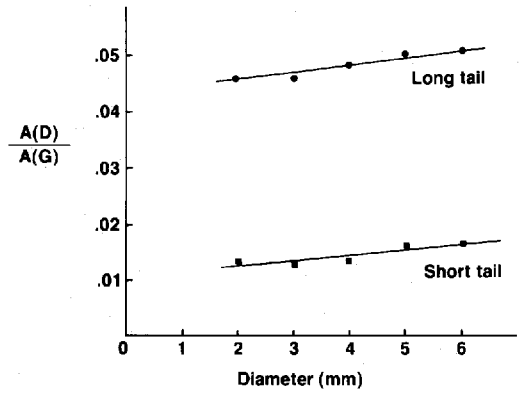


**Figure 3.** Tail/Gaussian intensity ratios for the scandium K$\alpha_1$ line as a function of aperture diameter.

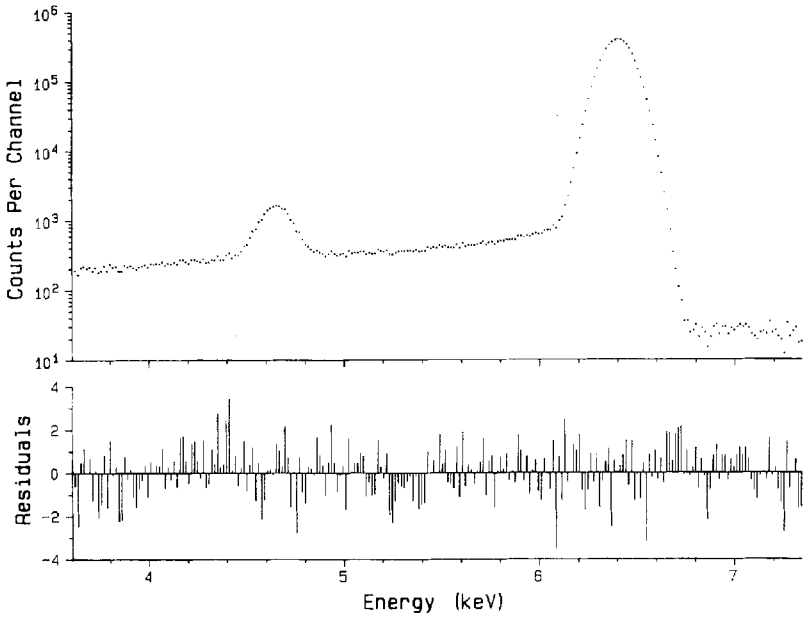


**Figure 4.** Results of final fit to the iron K$\alpha_1$ line using Eqn (7). The residues are weighted by the square root error of the counts per channel.

counts of 1.16, 1.07, 1.07, 1.06, 1.02, 1.02 and 1.12, respectively. A typical example is the Fe K$\alpha_1$ fit shown in Fig. 4.

Figure 5 shows that the relative areas contributed by each tail behave logarithmically as a function of photon energy. This well defined behaviour persists up to ca 20 keV for the long tail. For the short tail it persists up to ca 10 keV; at that energy the fitting program becomes unable to distinguish it from the widening Gaussian and starts to generate spuriously large short-tail intensities by 'stealing' events from the Gaussian. Evidence that this is the case is found in the very small values generated by the fits for the $\beta/\sigma$ value of the short tail; these imply that the short tail is almost Gaussian in shape, corresponding closely to, and scarcely displaced from, its Gaussian parent. Since by 10 keV, the ratio $A(D_S)/A(G)$ is *ca* 0.1%, it is a good tactic to omit it at higher energy.

For Ag L$\alpha_1$ at approximately 3 keV (Fig. 6), additional features are observed, which we confirmed by recording proton-induced K x-ray spectra from chlorine and sulfur. The main feature is a broad hump between the main peak and the escape peak; presumably this is simply part of the overall long-term tailing, which is so small as to be insignificant at higher energies ($E \geqslant 4$ keV). To describe it we added a Gaussian to the model of Eqn (7). Below the escape peak there is a well defined shelf, clearly associated with the escape peak; hence, for Ag L$\alpha_1$ the escape peak is described by a Gaussian with its own subsidiary left-hand shelf (complementary error function). This modified function gave an excellent fit (Fig. 6) with $\chi_r^2 = 1.05$ per $10^6$ counts, and the relative areas of the two tails (the long one redefined to include the extra Gaussian) agreed well with the trend established at higher energies.

The various height and slope parameters in the 3–12 keV region behave smoothly with varying energy, within their fairly large error limits. We have not produced a polynomial parameterization of the four energy dependences (Figs 7 and 8) since this is clearly a relatively trivial matter. The points to be stressed are (a) that such a parameterization, when effected, will allow the incorporation of detector tailing when fitting multiplets or complex spectra and (b) that the parameters are strongly energy dependent. The increase in uncertainty in the slope parameters as energy increases reflects the rapidly decreasing tail intensities.

## Escape peaks

In our previous paper[1] we simply demonstrated that the intensity ratio $A(E)/A(G)$ agreed fairly well with the

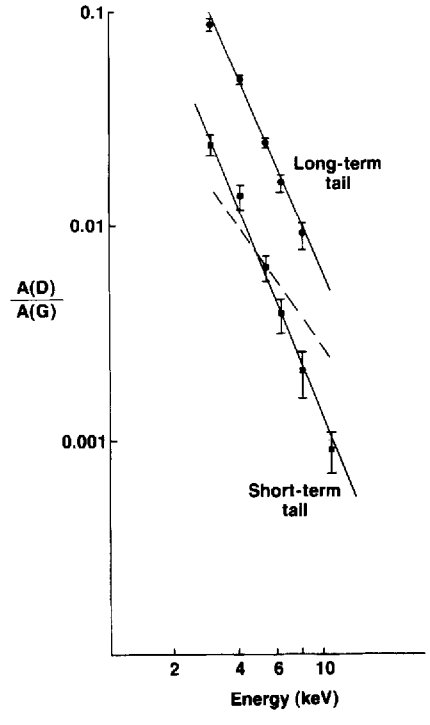


**Figure 5.** Tail/Gaussian intensity ratios deduced from fits of Eqn (7) to measured x-ray lines. The dashed line is predicted from the electron escape model of Shima *et al.*[6]

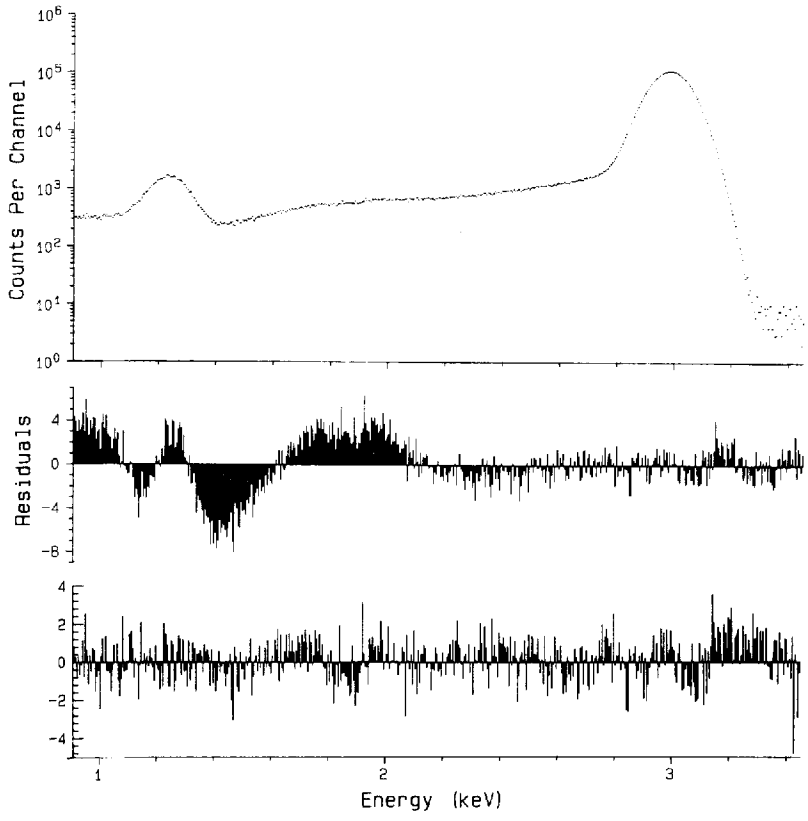


**Figure 6.** Results of the final fits to the silver $L\alpha_1$ line. The residues are weighted by the square root error of the counts per channel. See the text for detail regarding necessary modification of Eqn (7).

calculated values of Johansson.[3] Here we concentrate on the escape peak energy and lineshape.

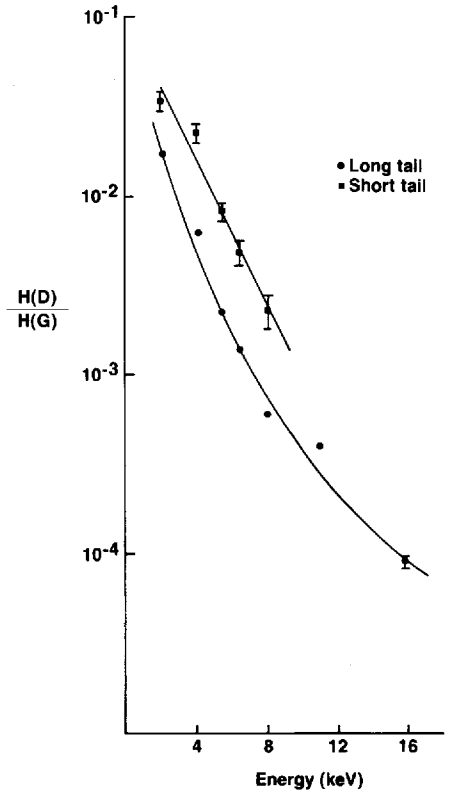


**Figure 7.** Energy dependence of the heights (relative to the Gaussian height) of the two tail components.

The escape peak energy was determined in three long runs, where $15 \times 10^6$ counts were accumulated in the fitting regions. Measurement of this energy required accurate calibration. This was afforded automatically by the presence in the spectrum of the second-order diffraction peak corresponding to photons from the white spectrum having an energy precisely twice that of the $K\alpha_1$ line under study. The system linearity was checked in two ways. Firstly, the standard approach of injecting

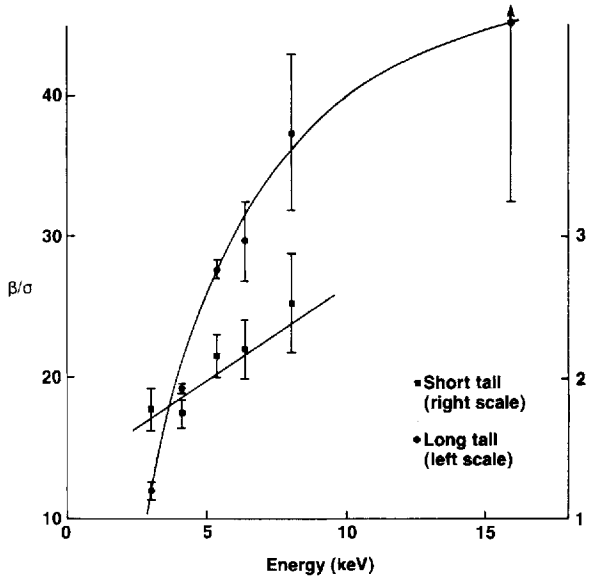


**Figure 8.** Energy dependence of the slopes (relative to the Gaussian width parameter $\sigma$) of the two tail components.

a very slowly rising linear ramp (from a BNC GL-3 pulser) and observing deviations from flatness in the resulting spectrum was used. Secondly, the first four harmonics of Cu K$\alpha_1$ were used to check the linearity of the energy versus centroid relationship. No statistically meaningful non-linearities were observed, and the error in escape peak energy from this source was much less than the error given by the fitting code.

The escape peak energies in Table 1 agree closely, with a mean of $1.752 \pm 0.002$ keV, significantly larger than the commonly adopted value of 1.742 keV. This result supports the earlier observation of this effect by Van Espen *et al.*[4]

The quality of fits indicates that it is worthwhile, if intensities are high, to adduce tailing to the escape peak. One would expect the escape peak tailing to be more intense than that of its parent, which is why our use of common tail parameters does not give a perfect fit. However, this is certainly superior to neglect of tailing. We speculate that if the appropriate tailing function were used, the escape energy might emerge as 1.742 keV; in other words, the apparent energy shift may simply reflect our inadequate description of the escape peak asymmetry. This is supported by the observation that total neglect of escape peak tailing leads to even larger escape energies in this detector.

### Measurement of dead layers

Various authors have described the front surface of an Si(Li) detector as consisting of a true dead layer in which there is zero charge collection and a second, thicker partially dead layer of incomplete charge collection. The latter will play some role (see below) in generating peak tailing, and if an appropriate model is used its thickness can be derived from the tailing. Manufacturers, on the other hand, generally specify one 'dead layer' of 0.1 μm thickness.

The thickness of the true dead layer can be determined via the measured intensity of silicon K x-rays fluoresced by low-energy photons of defined energy. We used a total detected intensity of $5.75 \times 10^6$ Sc K$\alpha_1$ x-rays (from the monochromator) and observed no Si K x-rays. The resultant upper limit for the true dead layer thickness is 0.027 μm at the 99% confidence level.

## DISCUSSION

We shall consider the above results in the context of recent work by Gardner *et al.*[5] and by Shima *et al.*[6] The latter workers were the first to derive a simple analytic model for the tailing intensity (relative to the main Gaussian area) to be expected from escape of both K- and L-shell Auger electrons and photoelectrons. [In retrospect it is remarkable that this problem was not treated much earlier in the history of Si(Li) detectors, as was the analogous problem of Si K x-ray escape.] In evaluating the predictions of Shima *et al.*'s model, we noted that the factor $(1-\omega_K)$ was erroneously omitted from Eqn (6) (cf. Ref. 6). Shima *et al.*[6] observed that the overall tailing intensity (obtained simply by counting channel contents left of a peak) was much larger than that predicted by their model for two detectors, but similar for a third. They deduced that other processes, such as the escape of thermal electrons (which are the end product of a photoelectric interaction) were in play to varying extents in these detectors.

By regarding the entire surface region from which electrons may be lost as a 'partially dead' layer of thickness $d$, and setting

$$\frac{N_t}{N_G} = \frac{1 - e^{-\mu^* d}}{e^{-\mu^* d}} \tag{8}$$

where $N_t$ = total tail intensity, $N_G$ = Gaussian intensity and $\mu^*$ = linear attenuation coefficient of silicon, Shima *et al.*[6] deduced $d$ values of 0.05, 0.1 and 0.2 μm for their three detectors.

In Fig. 5 the dashed line is the prediction of the model of Shima *et al.*[6] Its slope does not correspond to that of our short-term tail, but its area is of the same order. Hence there is some incentive, certainly not overwhelming, to identify our short tail as arising from escape of Auger electrons and photoelectrons. It may be that a better treatment of low-energy electron 'ranges' in Shima *et al*'s model would result in improved agreement. It is interesting that the energy dependences of the Auger electron and photoelectron contributions to the prediction are very different, so that slight changes could significantly alter the slope of the prediction in Fig. 5.

Gardner *et al.*[5] reported Monte Carlo computations of the tail intensity and spectral shape that result from K photoelectron and K Auger electron escape. Their simulation is found to exhibit the combined flat plateau and long-term exponential features that are observed experimentally; however, the simulated spectrum is at least one order of magnitude less than the corresponding experimental features, suggesting that other degradation processes were predominant in their detector. Gardner *et al.* suggest that L-shell photoelectron and L Auger electron escape could explain the short-term exponential tail.

Obviously our very tentative identification (via Shima *et al.*'s model) of our short-term tail as the result of electron escape is not consistent with the predictions of Gardner *et al.*

If the short-term tail were to be identified crudely as a partially dead layer without consideration of the mechanism of charge loss its thickness may be calculated from Eqn (8). The results are given in Table 2. If the effect were indeed due to such a layer, the derived $d$ values would be equal; their increase with increasing energy suggests that matters are more complex. For small $\mu^* d$, the right-hand side of Eqn (8) reduces to $\mu^* d$; using the parameterization of Leroux and Thinh[7] for the mass attenuation coefficient $\mu = \mu^*/\rho$ in terms of

**Table 1. Measured escape peak energies**

| Line | Line energy (keV) | Escape peak energy (keV) |
|---|---|---|
| Sc K$\alpha_1$ | 4.0906 | $1.7527 \pm 0.0006$ |
| Cr K$\alpha_1$ | 5.4147 | $1.7525 \pm 0.0006$ |
| Cu K$\alpha_1$ | 8.0478 | $1.7513 \pm 0.0006$ |

**Table 2. Thickness of 'partially' dead layer deduced from short-term tail intensity using Eqn (8)**

| Photon energy (keV) | Dead-layer thickness (μm) |
|---|---|
| 2.984 | 0.106 |
| 4.0906 | 0.142 |
| 5.4147 | 0.143 |
| 6.404 | 0.143 |
| 8.0478 | 0.151 |
| 10.98 | 0.160 |

photon energy $E$, and applying Eqn (8) to the short tail:

$$\ln \frac{A(D_S)}{A(G)} = \ln (C\rho d) - n \ln E \qquad (9)$$

where $C$ is a constant. The value of $n$ is given in Ref. 7 as 2.734 for $E < 5.9$ keV and 2.94 for $E > 5.9$ keV. Our measured slope of $2.47 \pm 0.16$ is slightly lower, again suggesting a more complex origin for the short tail than just a simple silicon dead layer.

These observations are in qualitative accord with the electron escape model; in this context there is no question of a defined thickness; the depth from which Auger electrons and photoelectrons escape increases with increasing photon energy.

To be consistent with this interpretation of the short tail, we would have to assume that the long tail arises from the near-surface region in which ionization charge is lost via thermal electron loss to the front surface or via surface channels to the edges. Using Eqn (8) the results give an approximate thickness of 0.50 μm for this region. Again, however, this should be treated very tentatively. The long-term tail undoubtedly does not retain its exponential nature all the way to zero energy, and so our use of the area under the fitted exponential is an approximation. The $n$ value observed here for the long tail is $2.28 \pm 0.08$.

## CONCLUSIONS

This study of Si(Li) detector lineshapes has shown that a Gaussian with two Gaussian-convoluted exponential tails is appropriate at photon energies above 4 keV. Below 4 keV the longer term tail becomes slightly convex upwards, and can be fitted by adding a broad Gaussian (of small intensity) to the exponential.

The height and slope parameters of the tails, expressed as multiples of the Gaussian height and width, are smoothly varying functions of energy. The relative fractions of peak area contained in the tails decrease smoothly with increasing energy. At $E > 10$ keV the tail intensities have become so small that our non-linear least-squares code no longer generates acceptable values (i.e. consistent with the trend at $E < 10$ keV) of tail parameters.

We observe a crude, semi-quantitative agreement between the measured area fraction in the short-term tail and the predictions of an analytic model based on escape of Auger electrons and photoelectrons. If these processes are indeed responsible for the short tail, then a similar energy dependence of that tail's intensity should be observed in other detectors. This would not be so for the long-term tail, to which this line of reasoning would consign all other charge collection deficiencies, which vary from detector to detector.

The fact that the sum of two Gaussian-convoluted exponentials describes the total tailing very accurately does not imply that each individual exponential is automatically the appropriate representation of a particular physical process. The identification of the short-term tail generated here with electron escape processes is very tentative indeed. It needs to be tested in detectors where long-term tailing is much decreased relative to our case.

We therefore plan further studies of monoenergetic photon lineshapes in other Si(Li) detectors. Since the hump that grows on the long-term tail at very low energies may carry information on the processes responsible for the long tail, these studies will make increased use of $L\alpha_1$ lines in the 2–4 keV region; it would also be desirable to employ $K\alpha_1$ lines (e.g. of Mg, Al, Si) whose energies lie below the silicon K absorption edge at 1.84 keV. To this end, our monochromator, which is currently very difficult to use at energies below 4 keV, is being rebuilt.

**Acknowledgement**

We are indebted to the Natural Sciences and Engineering Research Council of Canada for financial support.

## REFERENCES

1. J. L. Campbell, B. M. Millman, J. A. Maxwell, A. Perujo and W. J. Teesdale, *Nucl. Instrum. Methods* **B9**, 71 (1985).
2. G. W. Phillips and K. W. Marlow, *Nucl. Instrum. Methods* **137**, 525 (1976).
3. G. I. Johansson, *X-Ray Spectrom.* **11**, 194 (1982).
4. P. Van Espen, H. Nullens and F. Adams, *X-Ray Spectrom.* **9**, 126 (1980).
5. R. P. Gardner, A. M. Yacout, J. Zhang and K. Verghese, *Nucl. Instrum. Methods* **A242**, 399 (1986).
6. K. Shima, S. Nagai, T. Mikumo and S. Yasumi, *Nucl. Instrum. Methods* **217**, 515 (1983).
7. J. Leroux and T. P. Thinh, *Revised Tables of X-Ray Mass Attenuation Coefficients.* Corp. Scientifique Claisse, Québec (1977).